THE ASTROPHYSICAL JOURNAL, 393:729–741, 1992 July 10

ECLIPSE MAPS OF THE ACCRETION DISK IN THE CLASSICAL NOVA V PERSEI

JANET H. WOOD[1]
Institute of Astronomy, Cambridge, England, and Department of Astronomy, University of Texas at Austin, Austin, TX 78712
TIMOTHY M. C. ABBOTT
Department of Astronomy, University of Texas at Austin, Austin, TX 78712
AND
ALLEN W. SHAFTER
Department of Astronomy, San Diego State University, San Diego, CA 92182
Received 1991 July 8; accepted 1992 January 21

ABSTRACT

The surface brightness distribution in the accretion disk of V Per is reconstructed using a maximum entropy technique. The resulting brightness temperature gradient is much less steep than that from a standard steady state, optically thick disk for all reasonable mass accretion rates. A model including a rim which obscures part of the disk does not resolve this discrepancy. However, if the inner disk is disrupted out to $R_{in} \sim 0.15$–$0.25 R_{L1}$ (for example by a magnetic field), the brightness temperature gradient can be very close to a $T_b \propto R^{-3/4}[1 - b(R_{in}/R)^{1/2}]$ law. The value of R_{in} needed to match this steady state distribution depends on the distance to the system, its size and brightness, and the rotation rate of the white dwarf.

Subject headings: accretion, accretion disks — binaries: eclipsing — novae, cataclysmic variables — stars: individual (V Persei)

1. INTRODUCTION

V Per (Nova Persei 1887) is a relatively obscure cataclysmic variable with a quiescent visual magnitude of ~ 18. Interest in V Per was heightened recently with the discovery that the system eclipses with a period of 2.57 hr (Shafter & Abbott 1989). Aside from being one of the few deeply eclipsing novae (BT Mon, DQ Her, QZ Aur, and WY Sge being the others), V Per is particularly noteworthy in that its orbital period lies in the middle of the "gap" in the orbital period distribution of cataclysmic variables (see, e.g., Verbunt 1984). Shafter & Abbott (1989) have discussed possible evolutionary scenarios that could have brought V Per to this orbital period under the assumption that the system has evolved into the gap from a longer period. It is also possible that V Per was initially formed with a period already in the gap.

There are now two other cataclysmic variables known near the middle of the period gap: 1H 0709 − 360 (Tuohy et al. 1990) and V795 Her (Shafter et al. 1990). The former system is an intermediate polar (Tuohy et al. 1990), and the latter may be as well (Zhang et al. 1991). In this paper we use the term "intermediate polar" in its nonrestrictive sense, i.e., to represent any system where the inner part of the accretion disk is disrupted by the magnetic field of the white dwarf. Intermediate polars can be identified by the presence of coherent photometric oscillations caused by the nonsynchronous rotation of the white dwarf and are often X-ray sources. Based on the strength of the He II emission (4686 Å > Hβ, and a detection of the normally absent 5411 Å), Shafter & Abbott (1989) have suggested the possibility that V Per could also be an intermediate polar. It may be that intermediate polars do not have a gap in their orbital period distribution. Unfortunately, the number of known intermediate polars is presently insufficient to decide this question. The *ROSAT* survey should increase the sample size dramatically and allow a true picture of the orbital period distribution of intermediate polars to be determined.

The structure of the accretion disk varies from one type of cataclysmic variable to another. The accretion disks in high mass transfer rate systems, such as nova-like variables and classical novae, are expected to be very different to those in quiescent dwarf novae. Since their mass transfer rates are larger than the critical mass transfer rate for which the disk is stable, they are expected to be in a steady state and do not undergo quasi-periodic eruptions as dwarf novae do. The high mass transfer rate also serves to make the disks optically thick since their densities are higher than those in low mass transfer rate systems. The accretion disks in intermediate polars are expected to be disrupted to varying degrees, depending on the magnetic field strength of the white dwarf (see, e.g., the review by Lamb & Melia 1986). The inner disk radius may be much larger than the radius of the white dwarf. In one model for accretion in intermediate polars, King, Mouchet, & Lasota (1991) have suggested that the disks may not form at all.

A particularly powerful technique for studying the structure of accretion disks in cataclysmic variables is to use maximum entropy eclipse mapping for systems that eclipse. The structure of the accretion disk in several dwarf novae has been studied using the maximum entropy eclipse mapping method (e.g., Horne & Cook 1985; Wood et al. 1986; Warner & O'Donoghue 1988; Wood et al. 1989; and Wood, Horne, & Vennes 1991). Other types of cataclysmic variables have received less attention. Horne & Stiening (1985) studied the nova-like variable RW Tri, and Horne (1983) looked at several other nova-like systems including UX UMa, LX Ser, and V363 Aur and at DQ Her, an intermediate polar that is also a classical nova. Eclipse mapping of eclipsing intermediate polars (or suspected intermediate polars) will help to shed light on the accretion geometry in these systems.

In addition to studying differences between the subclasses of cataclysmic variables, it is also important to study possible

[1] Hubble Fellow.

variations in the structure of accretion disks in systems with different orbital periods. Such a study is related to the long-term evolution of cataclysmic variables as they evolve to shorter orbital periods, and to shorter term effects such as how they behave after nova explosions. Shara (1989) has reviewed the hibernation theory of novae. The theory predicts that the nova explosion causes the separation of the binary to increase. Hence, when the secondary star shrinks to its thermal equilibrium radius, mass transfer is much reduced or stops altogether until angular momentum loss decreases the separation again. The radiation from the nova explosion impinging on the secondary star keeps it larger than its thermal equilibrium radius for a few hundred years. Thus the mass transfer remains high for a few hundred years after the explosion. V Per is in this stage of post–nova evolution, as is DQ Her.

In this paper we use the light curves from Shafter & Abbott (1989) to reconstruct the surface brightness distribution of the disk in V Per using a maximum entropy eclipse mapping technique (Horne 1985). V Per is only the second classical nova, and the first cataclysmic variable in the period gap, to be investigated in this way. In addition to the usual assumption of a circular disk, we also consider the effects of a disrupted inner disk and an obscuring rim around the edge of the disk. We compare our results to those found in other cataclysmic variables and those expected from theoretical predictions.

2. MEAN LIGHT CURVES

Shafter & Abbott (1989) obtained six broad-band ("*BVR*") light curves of V Per using a CCD photometer (Abbott & Opal 1988) with a time resolution of 60 s (including 4 s dead time). This "*BVR*" bandpass covers the region 4000–9000 Å, with peak response at 6500 Å and effective wavelength 6000 Å. To reduce the flickering in the light curves and make more effective use of the eclipse mapping technique, we averaged these eclipses together.

When calculating the mean light curve we artificially increased the sampling of the original data to 1 s by linear interpolation between data points. We then phase-folded these light curves, using the ephemeris of Shafter & Abbott (1989), and rebinned the mean light curves to the original time resolution. The mean light curve is shown in Figure 1 with a measure of the uncertainty, as estimated from the variance of the individual cycles about the mean. In Table 1 we have tabulated the intensity of the mean light curve and 1 σ uncertainties for phase bins around the orbit. Smaller phase bins are used during eclipse than over the rest of the orbit. All intensities in this figure and table and elsewhere in this paper are given relative to a nearby comparison star, 15″ east and 7″ north of V Per.

We find no evidence for white dwarf or bright spot features in the mean light curve so we can apply the maximum entropy eclipse mapping technique directly. The flickering in the mean light curve of V Per is of very low amplitude and does not affect the eclipse mapping.

TABLE 1

INTENSITIES FROM MEAN LIGHT CURVE

Phase Bin	Intensity	σ
(−0.50, −0.40)	0.789	0.003
(−0.40, −0.30)	0.807	0.011
(−0.30, −0.20)	0.776	0.004
(−0.20, −0.10)	0.742	0.009
(−0.10, −0.08)	0.671	0.004
(−0.08, −0.06)	0.596	0.001
(−0.06, −0.04)	0.496	0.011
(−0.04, −0.02)	0.352	0.007
(−0.02, 0.00)	0.269	0.008
(0.00, 0.02)	0.256	0.004
(0.02, 0.04)	0.303	0.005
(0.04, 0.06)	0.411	0.001
(0.06, 0.08)	0.532	0.001
(0.08, 0.10)	0.640	0.003
(0.10, 0.20)	0.743	0.014
(0.20, 0.30)	0.758	0.007
(0.30, 0.40)	0.765	0.010
(0.40, 0.50)	0.759	0.006

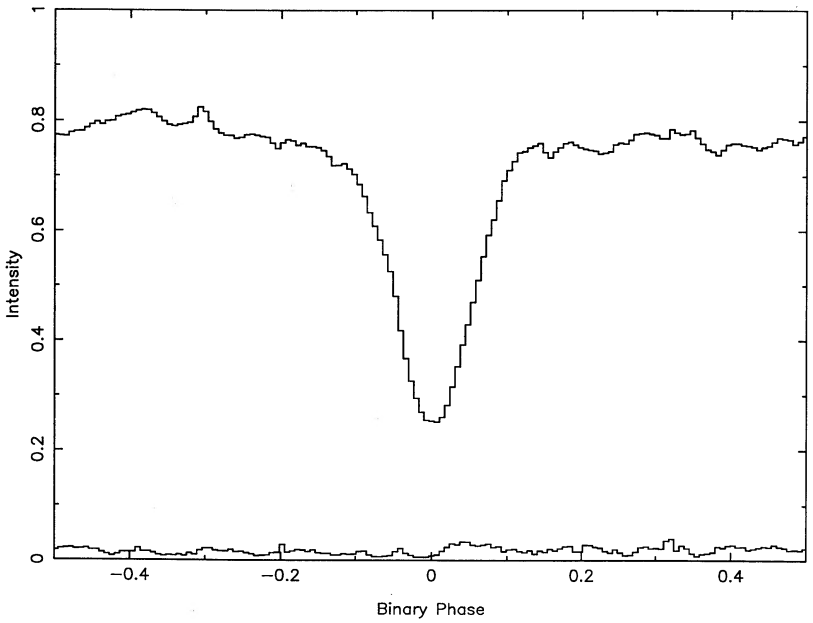

FIG. 1.—Mean *BVR* light curve of V Per at 60 s time resolution. The intensity is measured relative to a nearby comparison star.

3. SYSTEM PARAMETERS AND ECLIPSE GEOMETRY

Three geometrical parameters determine the shape of the eclipse for a particular surface brightness distribution: the phase of superior conjunction of the white dwarf (ϕ_0), the phase width of the eclipse of the center of the white dwarf ($\Delta\phi$), and the ratio of the mass of the secondary star and the white dwarf (q) (Horne 1985; Horne & Stiening 1985). The standard cataclysmic variable model assumes that the secondary star fills its Roche lobe; $\Delta\phi$ then provides a relationship between the mass ratio, q, and inclination, i.

The position of phase zero in the ephemeris, and hence in the mean light curve, corresponds to the position of minimum light. However, if the disk has any asymmetry, this need not correspond to ϕ_0, which therefore need not be zero. We found that the eclipse was most symmetric for $\phi_0 = 0.002$ and corrected the light curve phases by this amount.

For a given geometry (q, i, R_D), where R_D is the radius of the disk, all light curves for azimuthally symmetric brightness distributions will cross at the same point during ingress and egress (see Fig. 5 in § 4.1). To obtain a maximally symmetric map for a given q we must choose the value of i for which these crossing points lie on the observed light curve. Thus we do not assume any particular value for $\Delta\phi$, or measure it directly from the light curve, but can deduce it from our (q, i) pairs for comparison with those which would be determined by other methods.

The radius of the disk, R_D, can be estimated from the observed light curve using the phases at which the disk eclipse begins and ends (Sulkanen, Brasure, & Patterson 1981). The wider the eclipse, the larger R_D required. From the light curve of V Per we estimate $R_D = 0.75R_{L1}$ where R_{L1} is the distance from the center of the white dwarf to the L1 point. R_D/R_{L1} is relatively insensitive to the value of q; therefore we shall use this value of R_D in the following analysis for all mass ratios. We have very little information about the mass ratio so we shall calculate the disk maps for a range of q. The smallest possible mass ratio for V Per is 0.16, when $i = 90°$.

Since we know little about the secondary star in V Per, we also calculate disk maps for several possible values of $f_{\rm red}$; where $f_{\rm red}$ is the contribution of the secondary star to the observed light curve, measured in the same intensity units as the light curve. Since the observed disk light curve is different for each value of $f_{\rm red}$, the inclination needed for a given mass ratio is also different.

Errors in choosing i will cause changes in the front-back symmetry of the flux distribution of the disk (where the front is the part of the disk nearest the L_1 point), i.e., they can cause such asymmetries or reduce them if any are genuinely present. The maximum entropy eclipse mapping method of reconstructing the surface brightness distributions results in the most azimuthally symmetric maps that data and adopted geometry will allow (Horne 1985).

4. ECLIPSE MAPS OF THE DISK IN V PERSEI

Horne (1985) described the eclipse mapping technique for reconstucting the surface brightness distribution in accretion disks from the shape of their eclipses. The method assumes that the disk is flat and lies in the orbital plane. In this section we describe the calculation of the maps.

4.1. *Standard Disk Model*

We first calculated the eclipse maps of V Per assuming that no correction for background light was needed ($f_{\rm red} = 0.0$) and using a range of mass ratios $0.2 < q < 1$. In Figure 2*a*, *b*, and *c* we show contour plots of the brightness distributions for these maps with $q = 0.2$, $q = 0.5$, and $q = 1$, respectively. The resulting fits to the mean light curve are shown in Figure 3. The fits all have reduced χ^2 of 1 and are very similar. The required values of i and hence $\Delta\phi$ for each of these mass ratios are listed in Table 2.

TABLE 2

PARAMETERS USED IN FIGURES

Model	q	$\Delta\phi$	i	$f_{\rm red}$
a.....	0.2	0.0725	85°0	0.000
b.....	0.5	0.0725	77.7	0.000
c.....	1.0	0.0775	73.6	0.000
d.....	0.5	0.0875	81.1	0.100
e.....	0.5	0.1008	88.1	0.225
f.....	0.5	0.0875	81.1	0.000

The quantity $\Delta\phi$ is often measured directly from the light curve. Opinions vary as to the best measure of ϕ_i and ϕ_e, the phases of ingress and egress of the center of the white dwarf (and disk), and hence of $\Delta\phi = \phi_e - \phi_i$. Horne & Stiening (1985) favor measuring the phases at the steepest part of the eclipse or at the half-depth points in the light curve. Bailey (1990) also uses the phases of half-depth in the eclipse. The steepest parts of ingress and egress probably provide a good measurement of $\Delta\phi$ but can be difficult to determine. The correct flux depth at which to measure ϕ_i and ϕ_e depends on the geometry of the system. If the projected area of the occulting star on the disk is large enough that half the disk is eclipsed at ϕ_i and ϕ_e, then the half-flux points in the light curve are the correct points to measure and not the half-depth points of the eclipse. (Actually, the curvature of the limb of the secondary star projected onto the disk means that, when $i \neq 90°$, the half-flux points very slightly underestimate $\Delta\phi$.) If the geometry is such that part of the disk is never eclipsed, less than half the flux will be obscured at ϕ_i and ϕ_e and the half-flux phases offer a lower limit on $\Delta\phi$. An upper limit on $\Delta\phi$ for each value of q is found for $i = 90°$. There is no reason for ϕ_i or ϕ_e to occur at the half-depth points, though if the eclipse is very deep these can be close to the half-flux points. Bailey (1990) sometimes used the half-depth points to determine $\Delta\phi$ and i. This overestimates $\Delta\phi$ and consequently q and could therefore have produced the observed systematic bias toward low values of i. Measuring $\Delta\phi$ is further complicated by the presence of light sources other than the disk and white dwarf: if the secondary star contributes a significant amount of light in the bandpass observed this must be removed before the phases are measured.

For the lower mass ratio models the value of $\Delta\phi$ we obtained is equal to that which would be measured from the half-flux phases: 0.0725. For the high-mass ratio models, however, a slightly larger value was needed. This difference is required because in the low-mass ratio models the inclination is high enough that half the disk is eclipsed at ϕ_i and ϕ_e, whereas with a high-mass ratio the lower value of the inclination means that the back part of the disk is never eclipsed. The greater relative size of the secondary star on the higher mass ratio models, and hence the occulting area, is more than outweighed by the lower inclination. For no mass ratio did $\Delta\phi$ approach the value which would be measured from the half-depth phases of the eclipse ($\Delta\phi = 0.11$). This emphasizes the

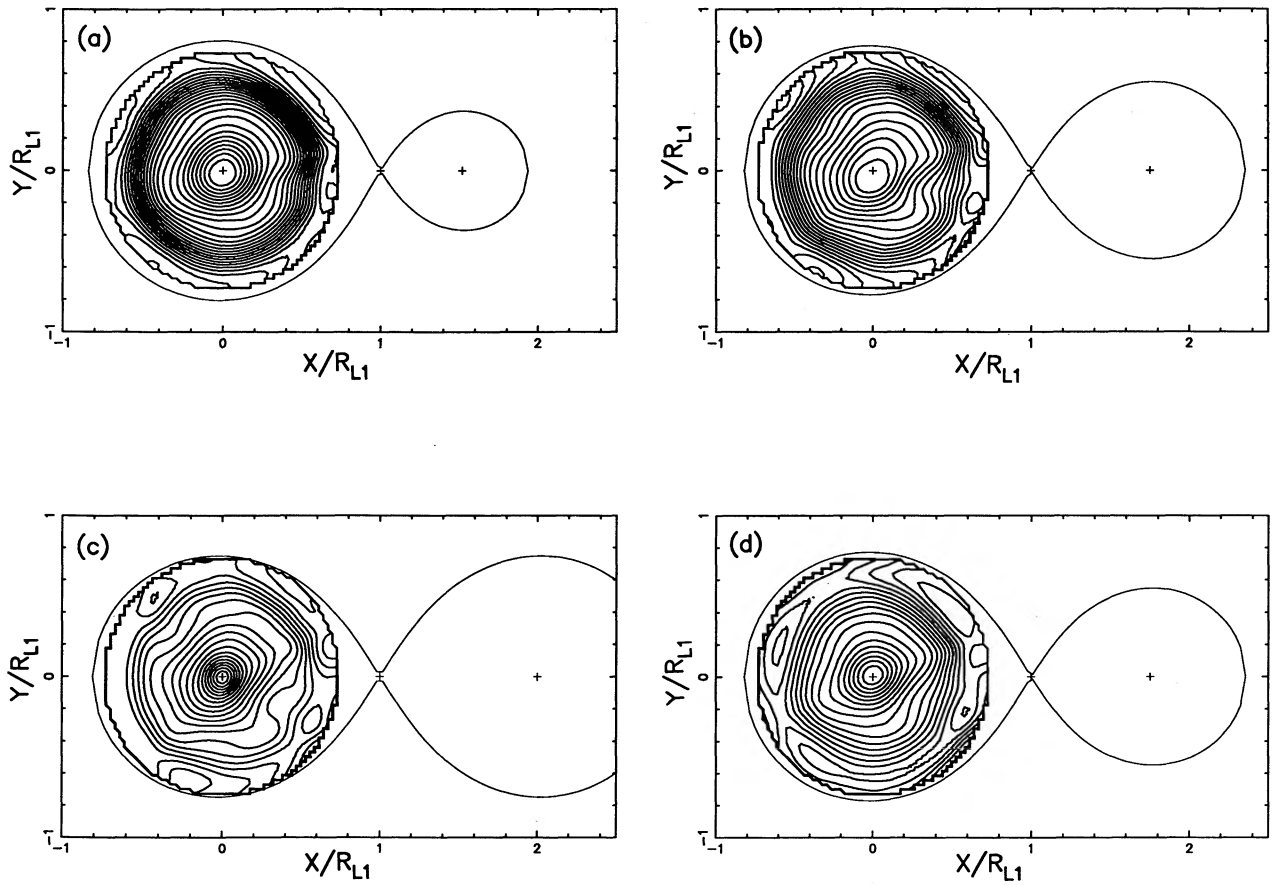

FIG. 2.—Eclipse maps of V Per. Contour plots on log scales with 0.025 decades between contours. (*a*) $q = 0.2$, $\phi_0 = 0.002$, $\Delta\phi = 0.0725$, $f_{red} = 0.0$. (*b*) $q = 0.5$, $\phi_0 = 0.002$, $\Delta\phi = 0.0725$, $f_{red} = 0.0$. (*c*) $q = 1.0$, $\phi_0 = 0.002$, $\Delta\phi = 0.0775$, $f_{red} = 0.0$. (*d*) $q = 0.5$, $\phi_0 = 0.002$, $\Delta\phi = 0.0875$, $f_{red} = 0.1$.

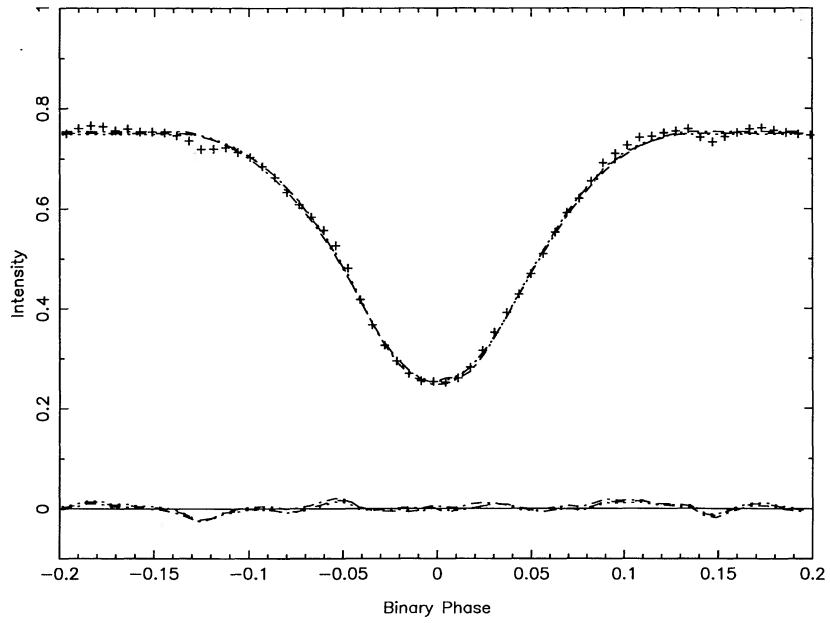

FIG. 3.—Fits to mean light curve of V Per for the eclipse maps in Fig. 2. The dashed line corresponds to the map in Fig. 2*a*, the dotted line to that in Fig. 2*b*, the dash-dotted line to the map in Fig. 2*c*, and the dash-dot–dash-dot line to that in Fig. 2*d* (after adding 0.1 to account for f_{red}).

fact that the half-depth phases should not be used to measure $\Delta\phi$ (as discussed above).

To compare our empirical maps of the brightness distribution with physical models, we implicitly define the brightness temperature T_b as

$$f_0 f = \frac{A}{D^2} \frac{\int c(\lambda) B_\nu(T_{br}, \lambda) d\lambda/\lambda}{\int c(\lambda) d\lambda/\lambda}, \quad (1)$$

where $c(\lambda)$ is the response function for the bandpass observed, A is the projected area in an elemental area of the disk, and D is the distance. The flux density, f, is measured in our intensity units but f_0 is the true flux density from the source divided by our uncalibrated flux density. Hence $f_0 f$ gives the true flux density in each pixel. The brightness temperature used here is the temperature of the blackbody which would produce the observed count rate in the bandpass defined by $c(\lambda)$.

Since the system parameters and distance to V Per are not known, and the data are uncalibrated, there is an unknown scaling factor in this equation. Equation (1) shows that all the uncertainties in the brightness temperature can be grouped together and treated as one unknown scaling factor, C, where $C = D^2 f_0/A$ mJy kpc^2 $R_\odot^{-2}$. We can then explore the range of possible brightness temperature distributions by calculating them for a wide range of this factor. In Figure 4 we plot as dots the brightness temperature distributions corresponding to the disk maps in Figure 2 for scaling factors of $C = 1$, 25, and 100 (the highest temperatures correspond to the largest scaling factor). The absolute brightness temperatures change significantly but the gradient varies by only a small amount.

If each element radiates as a blackbody, and the disk is optically thick and in a steady state, the brightness temperature at each radius in the disk is given by

$$\sigma T_b^4(R) = \frac{G M_{\rm wd} \dot{M}}{8\pi R^3} \left[1 - b\left(\frac{R_{\rm in}}{R}\right)^{1/2}\right] \quad (2a)$$

(Pringle 1981) or, equivalently,

$$\sigma T_b^4(R) = \frac{3\pi \dot{M} a^3}{2P^2(1+q)R^3} \left[1 - b\left(\frac{R_{\rm in}}{R}\right)^{1/2}\right], \quad (2b)$$

where $0 \le b \le 1$ depending on the rotation rate of the white dwarf, $M_{\rm wd}$ is the mass of the white dwarf, $R_{\rm in}$ the inner radius of the disk (taken to be the white dwarf radius), P the orbital period, and a the separation. Equating T_b from equation (1) with that of equation (2) relates the scaling factor C and the mass transfer rate, $\dot{M}$. However, we cannot give an explicit formula as T_b is obtained iteratively in equation (1). Shown as solid lines in Figure 4 are lines corresponding to the predicted brightness temperatures for steady state, optically thick models with various mass transfer rates. In Figure 4 we have used $R_{\rm in} = 0.012 R_{L1}$.

The uncertainties in the geometry of V Per produce uncertainties in T_b, as deduced from equation (2), which are insignificant compared to the uncertainties in the brightness temperatures caused by the unknown scaling factor. Thus we can estimate the possible range of scaling factors by comparing the resulting mass transfer rates with those expected in classical novae. Figure 4 shows that for our largest scaling factor the brightness temperatures correspond to a mass transfer rate of $\sim 10^{-7}$ $M_\odot$ yr^{-1} in the outer regions, which is slightly higher than expected ($\sim 10^{-8}$ $M_\odot$ yr^{-1} is more usual for a classical nova). Our smallest factor corresponds to mass transfer rates of $\sim 10^{-10}$ $M_\odot$ yr^{-1} which is lower than is expected for V Per (Shafter & Abbott 1989). We therefore believe that we have covered the entire range of possible distributions with our choice of scaling factors. Thus the gradients of the distribution are always much flatter than that of a steady-state, optically thick disk.

We then calculated the maps with corrections for background light from the secondary star with values of $f_{\rm red}$ between 0.0 and 0.225. Figure 2*d* shows the results obtained after a contribution $f_{\rm red} = 0.1$ was subtracted from the light curve. A mass ratio of 0.2 did not produce an eclipse wide enough to fit the data, so we show the map for $q = 0.5$ in Figure 2*d*. The geometry for this model is listed in Table 2 as model *d*. Figures 3 and 4*d* show the resulting fit and brightness temperature profiles. The brightness temperatures are a little lower for this map since the disk is fainter, but again the slope is much flatter than that expected for steady state, optically thick models. As q or $f_{\rm red}$ increase the maps become less steep and more asymmetric, especially in the outer regions. Although the absolute values of the brightness temperatures can vary, for all the eclipse maps that we calculated the gradient was extremely small.

We also tried the inverse procedure of assuming various steady state disk models and then calculating the expected light curves. We calculated them for disks with mass transfer rates of 10^{-4} $M_\odot$ yr^{-1}, 10^{-6} $M_\odot$ yr^{-1}, 10^{-8} $M_\odot$ yr^{-1}, and 10^{-10} $M_\odot$ yr^{-1} and $R_{\rm in} = 0.012 R_{L1}$. Each model is normalized to the light outside eclipse. In Figure 5*a* we plot the light curves for model *a* (Table 2). As discussed in § 3, the crossing points of the model light curves lie on the observed light curve. Figure 5*a* clearly shows that mass transfer rates of $\sim 10^{-4}$ $M_\odot$ yr^{-1} are required for a good fit to the light curve. For mass transfer rates smaller than this the predicted eclipses are too steep. Such a high mass transfer rate is not reasonable: the maximum possible mass transfer rate for which the accretion luminosity is below the Eddington limit is $\sim 10^{-5}$ $M_\odot$ yr^{-1}.

To investigate the effect assumptions about q, $R_{\rm in}$, and $f_{\rm red}$ have on the model light curves we calculated them for a range of parameters. We calculated eclipse light curves for other mass ratios between 0.2 and 1.0. As q increases the predicted eclipses become steeper and even the map corresponding to $\dot{M} = 10^{-4}$ $M_\odot$ yr^{-1} is too deep for $q > 0.2$. We varied the value of $R_{\rm in}$ from $0.010 R_{L1}$ to $0.025 R_{L1}$, when calculating the steady state maps but this small a range produced no significant differences. Only a small range of $R_{\rm in}$ is possible since it is determined here by the radius of the white dwarf. Finally we varied $f_{\rm red}$ between 0.050 and 0.225. Shown in Figure 5*b* are model light curves, normalized to the light outside eclipse after subtracting $f_{\rm red} = 0.225$ from the observed light curve. The geometry for this model is listed in Table 2 as model *e*. There is no good fit to the light curve for any $\dot{M}$ in this case. As $f_{\rm red}$ initially increases from 0.0, the predicted light curves become worse fits to the data. However, when $f_{\rm red}$ reaches 0.15 the map with $\dot{M} = 10^{-6}$ $M_\odot$ yr^{-1} produces a reasonably good fit. For $f_{\rm red} = 0.15$ the disk flux is 0.60 and therefore the secondary star would have to contribute one-quarter of the amount of light in the optical bandpass as the 10^{-6} $M_\odot$ yr^{-1} steady-state disk does. It is difficult to believe that the secondary star, which does not show up in the optical spectrum (Shafter & Abbott 1989), could contribute this much of the light.

It seems therefore that the simple steady state, optically thick solution is not possible with the standard disk model in V Per. The lack of such a solution is somewhat surprising in a system like V Per which appears to have a high mass transfer

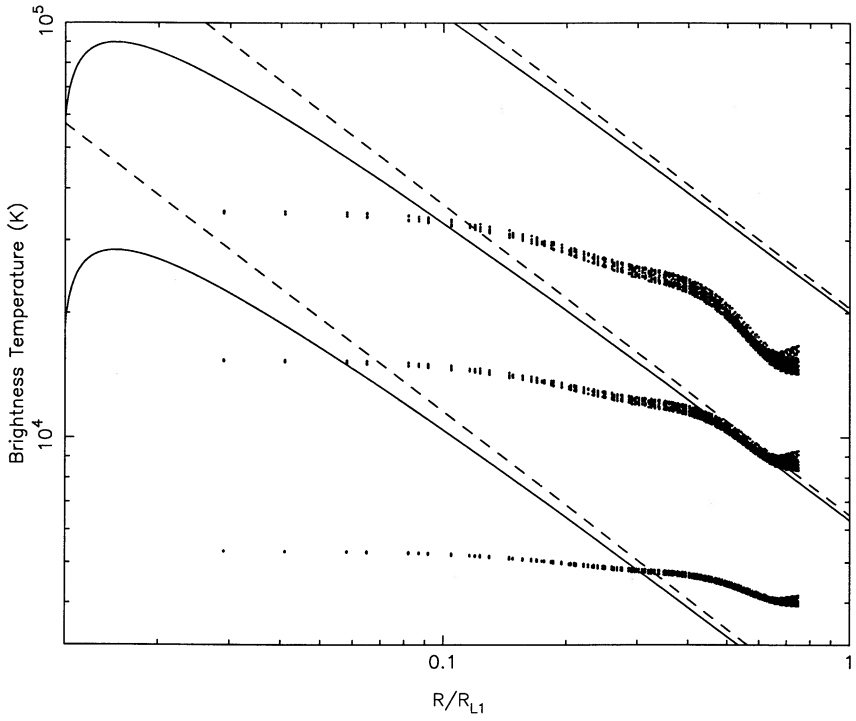

FIG. 4*a*

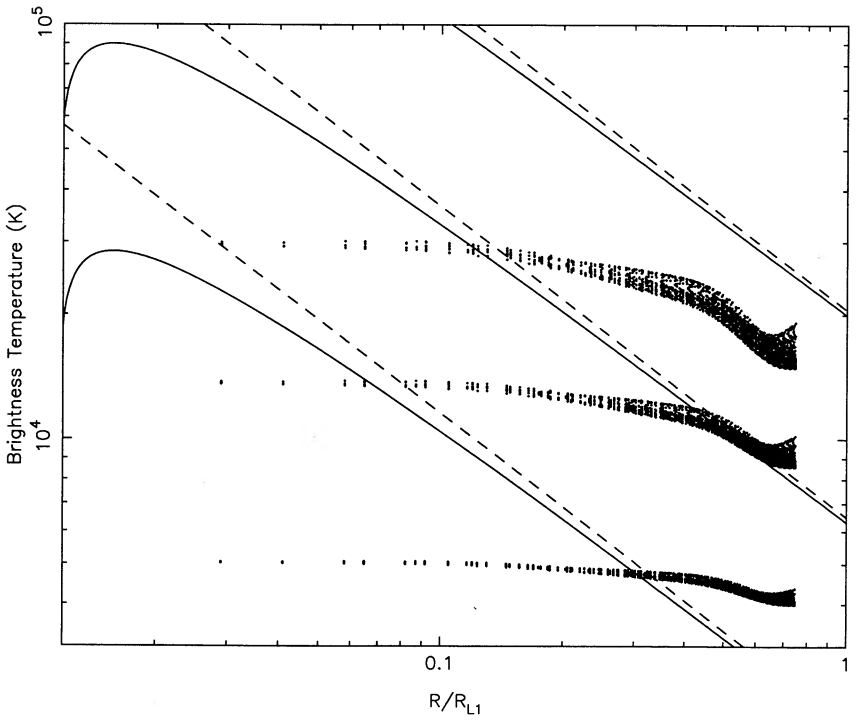

FIG. 4*b*

FIG. 4.—Brightness temperature profiles for the eclipse maps in Fig. 2. (*a*) $q = 0.2$, $\phi_0 = 0.002$, $\Delta\phi = 0.0725$, $f_{red} = 0.0$. (*b*) $q = 0.5$, $\phi_0 = 0.002$, $\Delta\phi = 0.0725$, $f_{red} = 0.0$. (*c*) $q = 1.0$, $\phi_0 = 0.002$, $\Delta\phi = 0.0775$, $f_{red} = 0.0$. (*d*) $q = 0.5$, $\phi_0 = 0.002$, $\Delta\phi = 0.0875$, $f_{red} = 0.1$. Also shown are steady state, optically thick models with $b = 0$ (*dotted lines*) and $b = 1$ (*solid lines*) for mass transfer rates of 10^{-10}, 10^{-8}, and $10^{-6}\ M_\odot\ \mathrm{yr}^{-1}$.

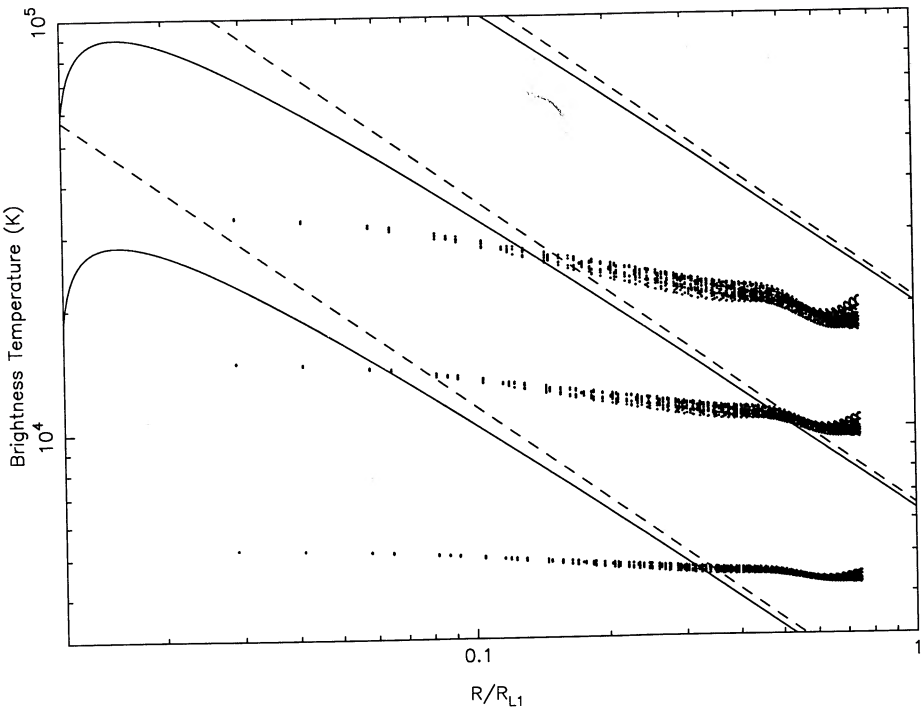

FIG. 4*c*

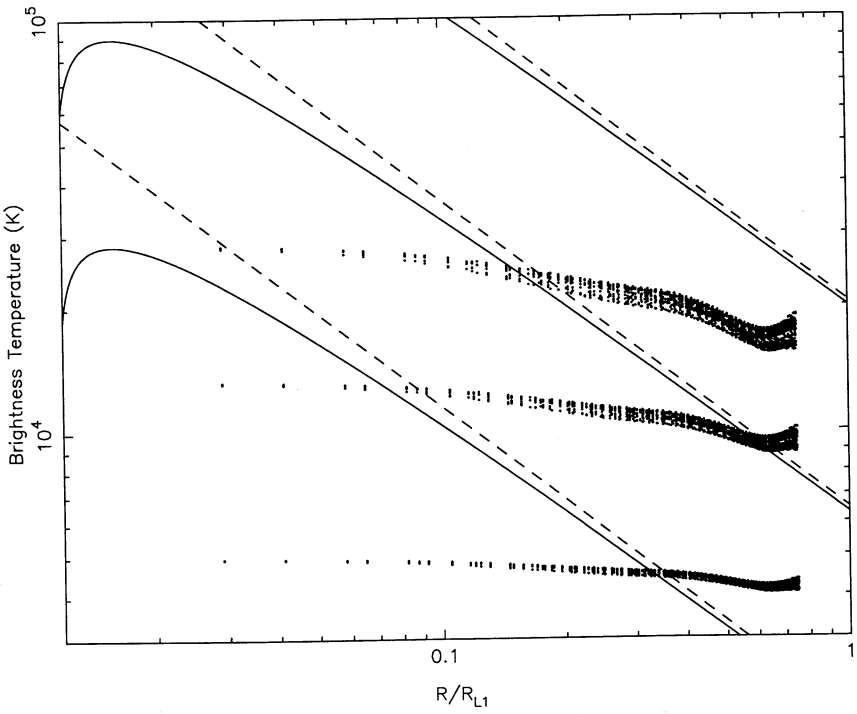

FIG. 4*d*

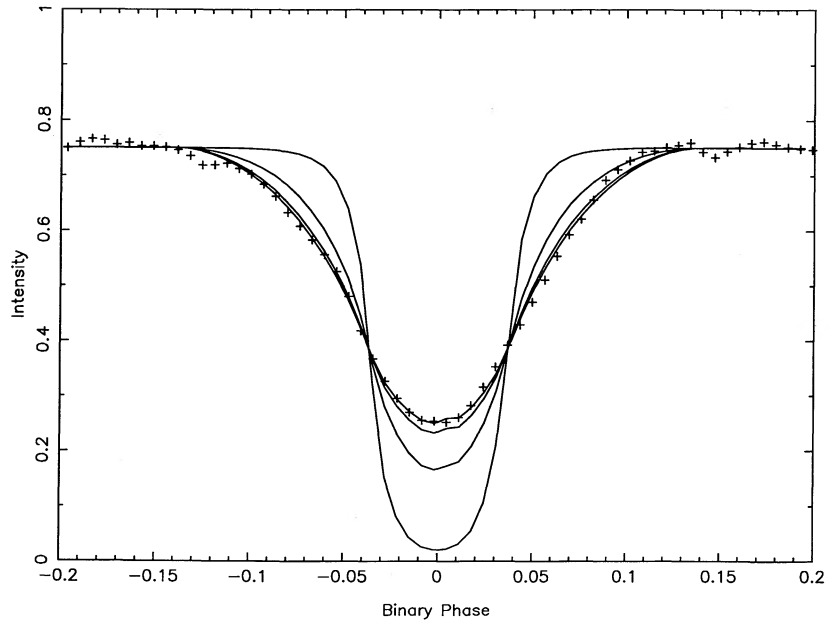

FIG. 5a

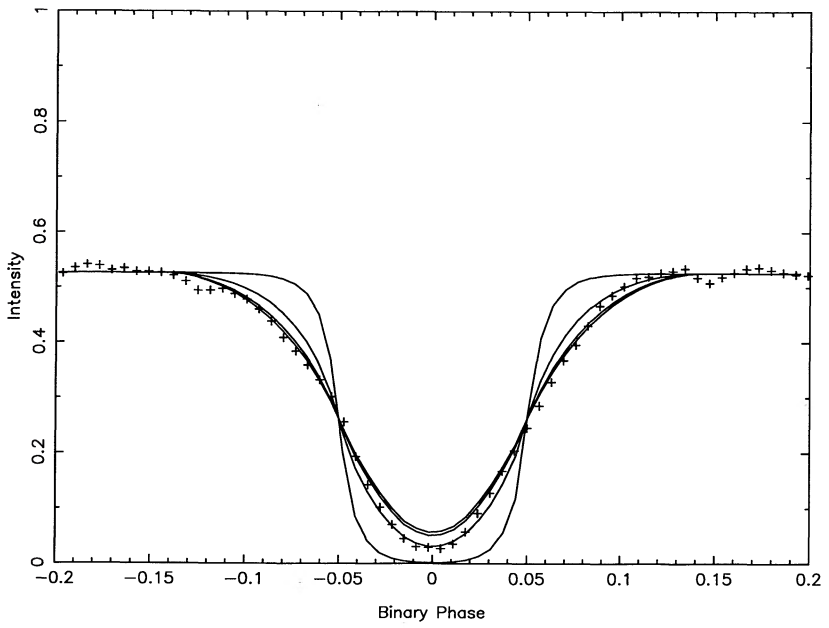

FIG. 5b

FIG. 5.—(*a*) Light curves of steady state, optically thick accretion disks, normalized to 0.751, for mass transfer rates of 10^{-10}, 10^{-8}, 10^{-6}, and $10^{-4}\ M_{\odot}\ \mathrm{yr}^{-1}$. The light curve of V Per is shown by the pluses. (*b*) Light curves of steady-state, optically thick accretion disks, normalized to 0.526, for mass transfer rates of 10^{-10}, 10^{-8}, 10^{-6}, and $10^{-4}\ M_{\odot}\ \mathrm{yr}^{-1}$. The light curve of V Per after subtracting $f_{\mathrm{red}} = 0.225$ is shown by the pluses.

rate (Shafter & Abbott 1989). This sort of cataclysmic variable, which has not been observed to undergo dwarf nova eruptions, is expected to have an optically thick and steady state disk. Low mass transfer rate systems such as the dwarf novae Z Cha and OY Car (Wood et al. 1986, 1989) also have very flat brightness temperature profiles but it is not unlikely that these systems are both optically thin and nonsteady. During a normal outburst Z Cha has a steep brightness temperature profile, very close to that of an optically thick, steady state disk (Horne & Cook 1985).

4.2. *Alternative Disk Models*

V Per has some unusual features: it underwent a nova eruption 100 yrs ago, it could be an intermediate polar, and it lies in the period gap. There is one confirmed eclipsing, intermediate polar which also had a nova eruption in the last hundred years; DQ Her (Nova Her 1934) (Ritter 1987). The orbital period of DQ Her is 4.65 hr. This system has been eclipse mapped by Horne (1983) and also shows a very flat brightness temperature profile. It is possible that either the nova explosion or the fact that these two systems are intermediate polars,

if indeed V Per is one, is causing the flat profiles. Unfortunately no eclipsing classical nova, which is definitely not an intermediate polar, has yet been mapped so we cannot compare our results with such a system. The eclipsing novae BT Mon (Ritter 1987) and QZ Aur (Shafter & Campbell 1991), however, would be excellent candidates for such a study. Other high mass transfer systems, e.g., RW Tri (Horne & Stiening 1985) and UX UMa (Horne 1983) have much steeper brightness temperature gradients.

If the mass transfer rate after a nova explosion were not steady, for example if it had been enhanced in the explosion and has been falling ever since (see the review of nova eruptions by Shara 1989), then the disks would not be in a steady state. However, as observations of outbursts of dwarf novae have shown (Horne & Cook 1985), the disk tends to go through a series of steady-state–like configurations. In outburst, when the mass transfer rate is high, the viscous time scale is such that the disk has time to achieve a steady state configuration before the mass transfer has changed significantly. Since the mass transfer rate is unlikely to be varying faster in V Per than in dwarf nova outbursts, we feel that this cannot be the explanation for the flat brightness profile in its disk.

It is, of course, possible that complicated processes, not included in the simple theoretical calculation, are occurring in the disk, e.g., removal of energy from the disk in a wind or the transport of energy via waves traveling through the disk. Such processes could significantly alter the temperature gradient in the disk.

4.2.1. *Disrupted Disk*

The fact that DQ Her is, and V Per may also be, a system where the magnetic field of the white dwarf is strong enough to disrupt the inner part of the accretion disk suggests another possible cause of a flat apparent brightness temperature distribution. In such systems the result might be approximated as an accretion disk with a hole in the middle. For a given surface brightness gradient, the eclipse shape of such a disrupted disk depends on how large the inner radius is relative to the outer radius. When the inner radius is large the eclipse will be more gradual and shallower than when it is small. It is possible that such a truncated disk could exist in V Per, hence we now recalculate the disk maps for V Per, using model *a*, with various inner radii.

Figure 6 shows the resulting surface brightness distributions for disks assumed to have inner radii of $0.15R_{L1}$ and $0.25R_{L1}$. Figure 7 shows the fits to the light curves these disks produced and Figure 8 the brightness temperatures (with the same scaling factors as before). The larger the inner radius, the steeper the brightness temperature gradient needed to fit the light curve. The theoretical predictions are also altered by the presence of the hole. Since the magnetic field that is disrupting the disk is rotating with the white dwarf, the boundary layer effectively occurs at the inner radius of the disk, R_{in}, instead of occurring at the white dwarf's surface, and therefore T_b is given by equation (2), where b now depends on the rotation rate of the magnetic field. We have plotted in Figure 8 lines showing the theoretical profiles expected for an optically thick, steady state disk with these inner boundaries for $b = 0$ and 1. Compared to an optically thick, steady state disk with $b = 1$, the disk map with $R_{in} = 0.15R_{L1}$ is still too flat for our lowest scaling factor, approximately the right gradient for the middle and slightly too steep for the highest. If $b = 0$ the highest scaling factor would be required. With $R_{in} = 0.25R_{L1}$ and

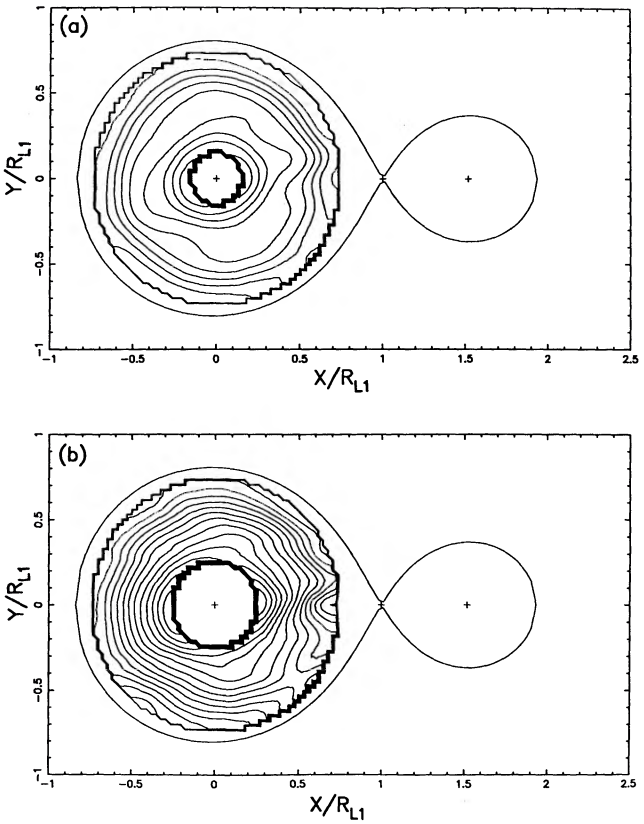

FIG. 6.—Eclipse maps of V Per with disk disrupted in the inner region, for $q = 0.2$, $\phi_0 = 0.002$, $\Delta\phi = 0.0725$, $f_{red} = 0.0$. The contours are logarithmic with 0.1 decades between contours. (*a*) $R_{in} = 0.15R_{L1}$. (*b*) $R_{in} = 0.25R_{L1}$.

$b = 1$ the slope is very close to the expected gradient for the lowest scaling factor and too steep for the others. The middle scaling factor would be the closest solution if $b = 0$. All these solutions correspond to much more reasonable mass transfer rates then could be obtained with steady state, optically thick models in § 4.1. Mass transfer rates of $\sim 10^{-8}$ to 10^{-7} $M_\odot$ yr^{-1} are needed for $R_{in} = 0.15R_{L1}$ and $\sim 10^{-9}$ to 10^{-8} $M_\odot$ yr^{-1} for $R_{in} = 0.25R_{L1}$. The critical mass transfer rate above which the disk in V Per is stable is $\sim 1 \times 10^{-9}$ $M_\odot$ yr^{-1} (see, e.g., Shafter, Wheeler, & Cannizzo 1986). Thus these results predict a stable disk, as is observed.

With an axisymmetric disk that has a large inner radius, kinks are produced in the light curve when the edges of the hole go into and out of eclipse. Since these features are not seen in the light curve of V Per the surface brightness distribution cannot be symmetric. The asymmetries in these maps are therefore more pronounced than in the previous maps. The disk in V Per could be optically thick and in a steady state if it has a disrupted inner disk with $R_{in} \sim 0.15$–$0.25R_{L1}$, depending on the scaling factor. It is important in the future to find out whether or not V Per is an intermediate polar, and hence if our model is plausible. If it is an intermediate polar this may be a requirement for a system to enter the period gap while still transferring mass. In general, a flat temperature profile in a cataclysmic variable known to have a high mass transfer rate could indicate that the cataclysmic variable has a disrupted inner disk.

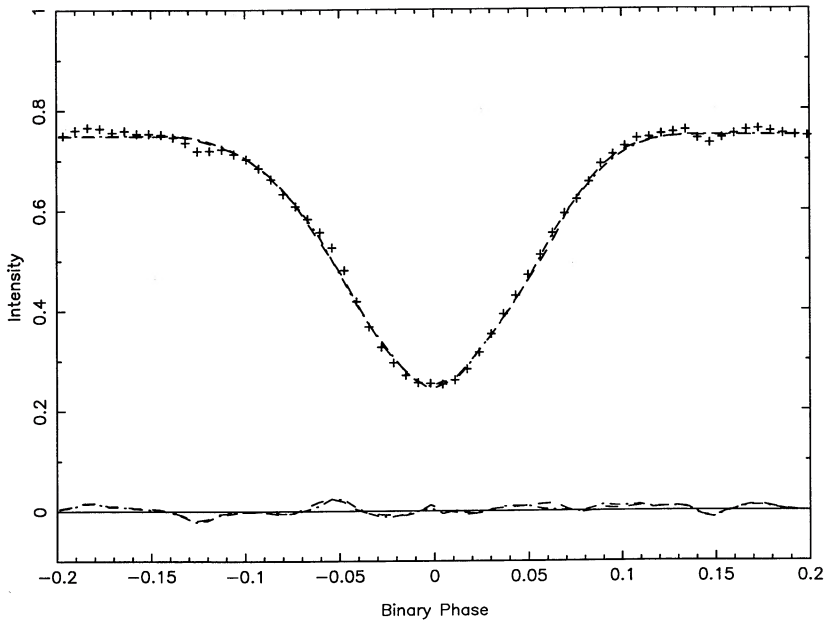

FIG. 7.—Fits to mean light curve of V Per for the eclipse maps in Figure 6. The dash-dot line corresponds to the map in Fig. 6*a*, the dotted line to that in Fig. 6*b*.

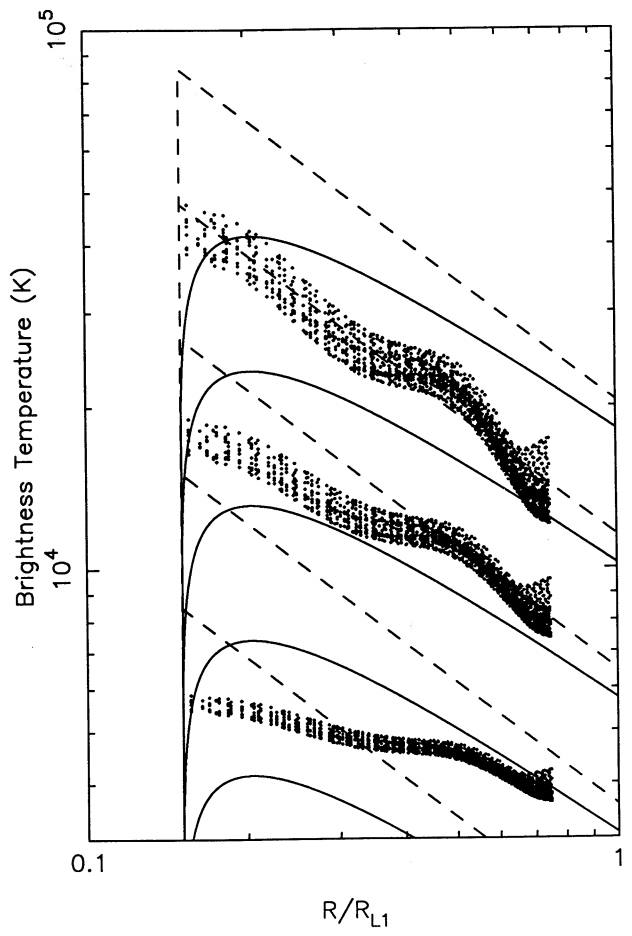

FIG. 8*a*

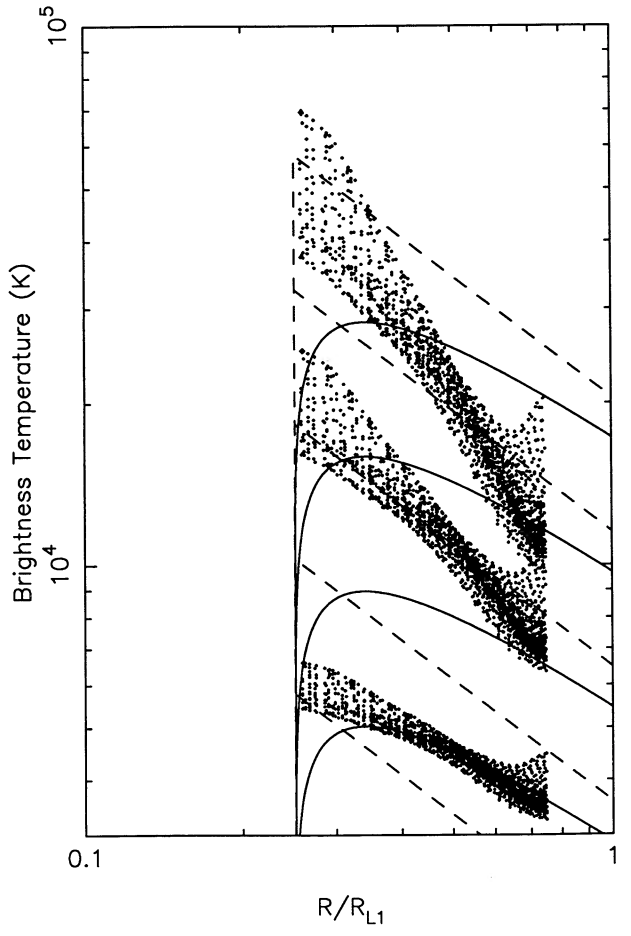

FIG. 8*b*

FIG. 8.—Brightness temperature profiles for the eclipse maps in Fig. 6. Also shown are lines with $T_b \propto R^{-3/4}\,[1 - b(R_{in}/R)^{1/2}]$, for $b = 0$ (*dotted lines*) and $b = 1$ (*solid lines*) and mass transfer rates of 10^{-10}, 10^{-9}, 10^{-8}, 10^{-7}, and $10^{-6}\ M_\odot\ \mathrm{yr}^{-1}$. (*a*) $R_{in} = 0.15R_{L1}$. (*b*) $R_{in} = 0.25R_{L1}$.

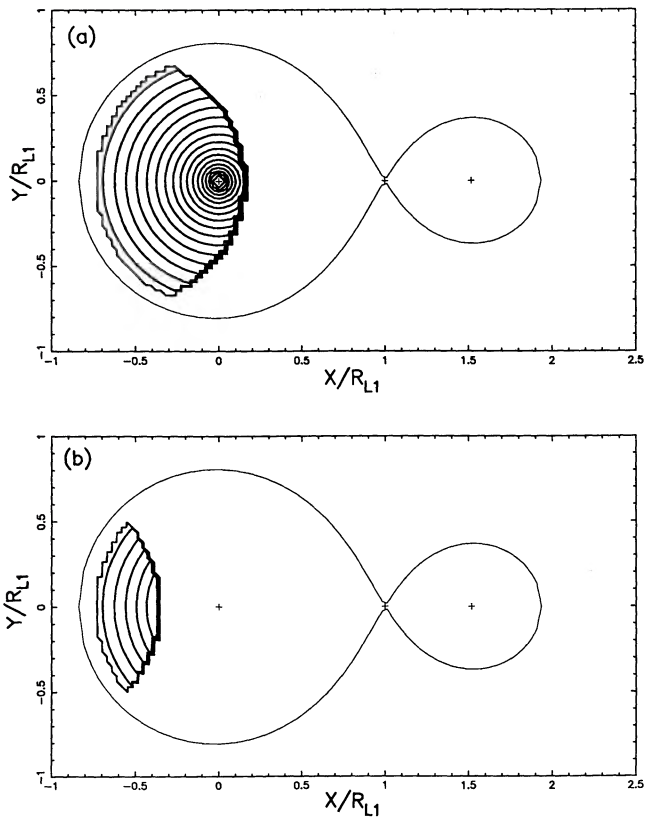

FIG. 9.—Contour plots of a steady state, optically thick disk with an obscuring rim on log scales with 0.1 decades between contours. (*a*) For $l = 0.6R_{L1}$. (*b*) For $l = 1.1R_{L1}$.

4.2.2. *Disk Rim*

Another possibility to consider is that high mass transfer rate systems, such as dwarf novae in outburst or superoutburst, classical novae, and novalike variables, may have a flared outer rim on their accretion disks (Naylor et al. 1987). At very high inclinations such a rim could obscure large parts of the disk and hence affect the observed shape of the eclipse and the inferred brightness temperature profile. We first consider totally dark rims of various heights. For V Per, a deeply eclipsing system, the inclination could be close to 90°. For a semi-thickness of the outer disk of $0.01R_{\rm out}$, with $R_{\rm out} = 0.75R_{L1}$ and $i = 89°.3$, this corresponds to a projection of length $l = 0.6R_{L1}$ on the disk at the point on the rim nearest the observer. Figure 9*a* shows a contour plot of the part of an optically thick, steady state disk unobscured by the rim for $l = 0.6R_{L1}$. Shown in Figure 9*b* is the same disk for $l = 1.1R_{L1}$.

In our previous calculations of eclipse light curves we have assumed that any asymmetries in the disks remained fixed with respect to the binary orbit. The projection of an obscuring rim on the disk remains fixed with respect to the observer and the visible part of the disk, as shown in Figure 9, effectively rotates with respect to the binary. The configurations shown correspond to phase 0.0. We note that a rim is not the only possible cause of an asymmetry that would follow the observer and not the binary. For example, the line of sight at the front of the disk, i.e., the half of the disk closest to the observer, first passes through cooler material and then hot whereas the situation is reversed at the back of the disk. This would be particularly important in an optically thin disk. To check if we had suppressed any such features in our previous disk mapping we recalulate the map in Figure 2*a* holding the disk brightness fixed relative to the observer instead of the binary. No significant changes were found. This was not surprising since the disk in V Per is expected to be optically thick and our original disk maps were fairly symmetric and thus give very similar light curves whether or not the surface brightness in the disk rotates with respect to the binary.

Shown in Figure 10*a* are the resulting eclipses, normalized to 0.751, for the disk plotted in Figure 9*a* and a disk with the same obscuration but a uniform brightness distribution. Again we chose $\Delta\phi$ such that azimuthally symmetric model light curves crossed on the observed light curve. Figure 10*b* shows the same models for $l = 1.1R_{L1}$. The geometry used in Figure 10 is listed as model *f* in Table 2. Also shown in Figure 10 are the light curve of V Per and the residuals each model gives to the light curve. The residuals from the steady state, optically thick models are shown as "+" and those corresponding to the uniform disk models as "□" Clearly the steady state, optically thick models cannot give a good fit to the observed light curve in V Per, even when including a dark rim. As l increases, the eclipse of a uniform disk becomes deeper but at the same time narrower. A disk fairly close to uniform brightness with $l \sim 0.6R_{L1}$ could produce the observed eclipses. The presence of a dark rim therefore does not help reduce the discrepancy between the expected steep temperature gradient and that required to fit the eclipse. Scaling a uniform distribution has no effect on the gradient and therefore this conclusion is not affected by the unknown scaling factor.

If the rim were uniform and bright, not dark, its presence would result in the addition of a wide, flat-bottomed eclipse to the model light curves shown in Figure 10. Obviously, since the observed eclipse is not flat-bottomed such a rim cannot dominate the light curve. Indeed, a funnel-shaped eclipse would be obtained by adding a bright rim to the obscured steady state disk. This is not seen; therefore we conclude that the presence of an obscuring rim, bright or otherwise, does not help to fit the observed eclipse shapes with a steady state, optically thick disk.

5 CONCLUSIONS

We have used a mean light curve to reconstruct the surface brightness distribution in the disk of V Per under a variety of assumptions. We find that the disk must have a much flatter brightness profile than that in the standard model of a steady state, optically thick disk with a reasonable mass transfer rate, unless the inner disk radius is large, $R_{\rm in} \sim 0.15$–$0.25R_{L1}$. This could occur if V Per contains a magnetic white dwarf, a possibility noted by Shafter & Abbott (1989). An obscuring outer rim on the disk does not help explain why the reconstructed brightness profiles are not as steep as expected. Although a disrupted disk is only one possible explanation for the flat temperature profiles, in the future it would be valuable to look for evidence that V Per may be an intermediate polar. For example, the light curve should be examined for periodicities other than the orbital period. The detection of V Per as an X-ray source would also strengthen the case that the system harbors a magetic white dwarf, though such a detection is not required for V Per to have a disrupted inner disk.

We wish to thank K. Horne, F. Verbunt, W. Bunk, C. Haswell, T. Naylor, and B. J. M. Hassall for helpful dis-

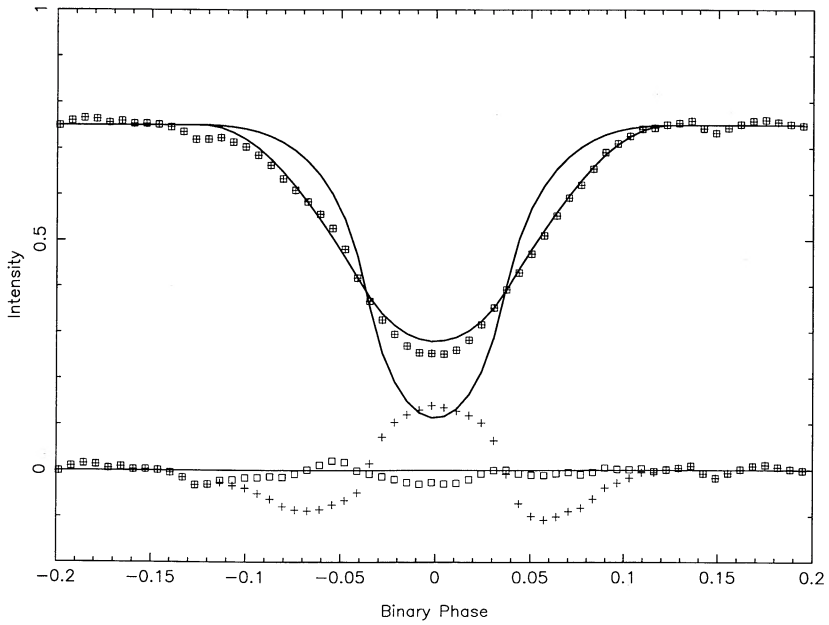

FIG. 10*a*

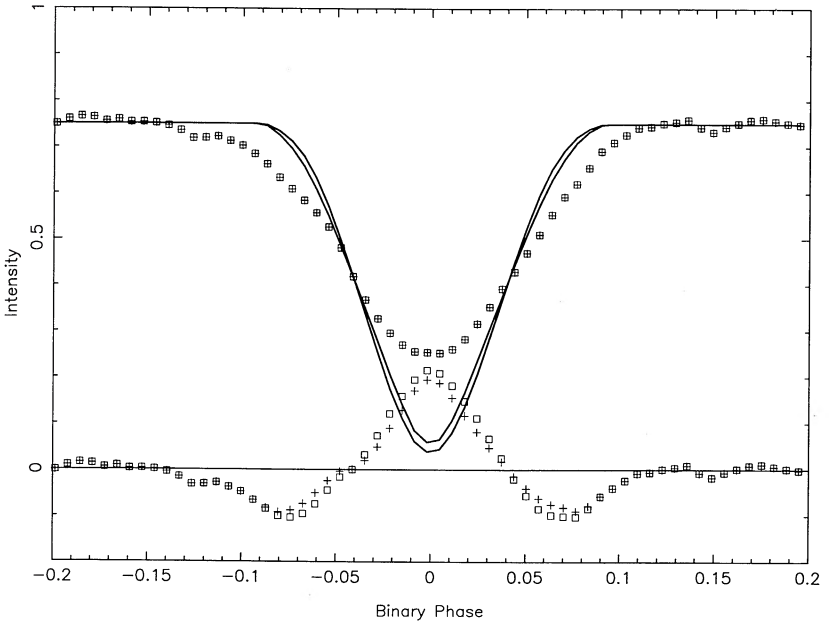

FIG. 10*b*

FIG. 10.—Light curves for $q = 0.5$ corresponding to a steady state disk with $\dot{M} = 10^{-8}\ M_{\odot}\ \mathrm{yr}^{-1}$ and a uniform disk, normalized to 0.751. The light curve of V Per is shown with the residuals from each model. Plus sign corresponds to the uniform model and □ to the steady state model residuals. (*a*) For $l = 0.6R_{L1}$. (*b*) For $l = 1.1R_{L1}$.

cussions. We are grateful to the referee for helpful comments on the manuscript. A. W. S. acknowledges partial support from NSF grant AST 8704382. J. H. W. is grateful to St. John's College Cambridge for a fellowship during part of this work. Partial support was provided by NASA through grant HF-1012.01-90A awarded by the Space Telescope Science Institute which is operated by the Association of Universities for Research in Astronomy, Inc., for NASA under contract NAS5-26555. The calculations were performed on the Cambridge node of the SERC STARLINK network using software originally developed by K. Horne and MEM routines by S. Gull and J. Skilling.

REFERENCES

Abbott, T. M. C., & Opal, C. B. 1988, in Instrumentation for Ground-Based Astronomy, ed. L. B. Robinson (Munich: Springer), 386
Bailey, J. 1990, MNRAS, 243, 57
Horne, K. 1983, Ph.D. thesis, California Institute of Technology
———. 1985, MNRAS, 213, 129
Horne, K., & Cook, M. C. 1985, MNRAS, 214, 307

Horne, K., & Stiening, R. F. 1985, MNRAS, 216, 933
King, A. R., Mouchet, M., & Lasota, J. P. 1991, in Structure and Emission Properties of Accretion Disks, ed. C. Berout, S. Collin-Souffrin, J. P. Lasota, & J. Tran Thanh Van (Paris: Editions Frontières), 213
Lamb, D. Q., & Melia, F. 1986, in The Physics of Accretion onto Compact Objects, ed. K. O. Mason, M. G. Watson, & N. E. White (Munich: Springer), 113
Naylor, T., Charles, P. A., Hassall, B. J. M., Bath, G. T., Berriman, G., Warner, B., Bailey, J., & Reinsch, K. 1987, MNRAS, 229, 183
Patterson, J. 1984, ApJS, 54, 443
Pringle, J. E. 1981, ARAA, 19, 137
Ritter, H. 1987, A&AS, 70, 335
Shafter, A. W., & Abbott, T. M. C. 1989, ApJ, 339, L75
Shafter, A. W., & Campbell, R. D. 1991, in preparation
Shafter, A. W., Wheeler, J. C., & Cannizzo, J. K. 1986, ApJ, 305, 261
Shafter, A. W., Robinson, E. L., Crampton, D., Warner, B., & Prestage, R. M. 1990, ApJ, 354, 708
Shara, M. M. 1989, PASP, 101, 5
Sulkanen, M. E., Brasure, L. W., & Patterson, J. 1981, ApJ, 224, 579
Tuohy, I. R., Remillard, R. A., Brissenden, R. J. V., & Bradt, H. V. 1990, ApJ, 359, 204
Verbunt, F. 1984, MNRAS, 209, 227
Warner, B., & O'Donoghue, D. 1988, MNRAS, 233, 705
Wood, J. H., Horne, K., Berriman, G., & Wade, R. A. 1989, ApJ, 341, 974
Wood, J. H., Horne, K., Berriman, G., Wade, R. A., O'Donoghue, D., & Warner, B. 1986, MNRAS, 219, 619
Wood, J. H., Horne, K., & Vennes, S. 1992, ApJ, 385, 294
Zhang, E. H., Robinson, E. L., Ramseyer, T. F., Shetrone, M. D., & Stiening, R. F. 1991, ApJ, 381, 534